LAWRENCE
LIVERMORE
NATIONAL
LABORATORY

LLNL-JRNL-441353

DENSITY-FUNCTIONAL STUDY OF BCC Pu-U, Pu-Np, Pu-Am, AND Pu-Cm ALLOYS

A. Landa, P. Soderlind, P. E. A. Turchi, L. Vitos, O. E. Peil, A. V. Ruban

July 12, 2010

Journal of Nuclear Materials

Disclaimer

Density-functional study of bcc Pu-U, Pu-Np, Pu-Am, and Pu-Cm alloys

A. Landa[1*], P. Söderlind[1], P. E.A. Turchi[1], L. Vitos[2,3], and O.E. Peil[2,4], and A.V. Ruban[2]

[1]Lawrence Livermore National Laboratory, Livermore, CA 94551, USA

[2]Royal Institute of Technology, SE-10044, Stockholm, Sweden

[3]Uppsala University, SE-75121 Uppsala, Sweden

[4]University of Hamburg, 20355 Hamburg, Germany

Abstract

Density-functional theory, previously used to describe phase equilibria in the γ-Pu-U-Zr alloys [A. Landa, P. Söderlind, P.E.A. Turchi, L. Vitos, A. Ruban, J. Nucl. Mater. 385 (2009) 68; *ibid.* 393 (2009) 141], is extended to study ground-state properties of the γ-Pu-Np, γ-Pu-Am, and γ-Pu-Cm solid solutions. Calculated heats of formation are compared with CALPHAD assessments where possible. We discuss how the heat of formation correlates with the charge transfer between the alloy components.

Keywords: nuclear reactor materials, phase transitions, first principles.

[*] Corresponding author. Tel.: + 1 925 424 3523; fax: +1 925 422 2851. E-Mail address: landa1@llnl.gov

1. Introduction

In our previous papers, Refs. [1, 2], we performed a detailed *ab initio* study of the fundamental thermodynamic properties of the γ-Pu-U-Zr system that is a candidate metallic nuclear fuel for fast breeder reactors. We found that calculated heats of formation of the body-centered-cubic (bcc) γ phases of U-Zr, Pu-U, and Pu-Zr alloys are in a good agreement with CALPHAD assessments and established that spin-orbit coupling is important for accurate descriptions of Pu-containing alloys.

Although Pu-U-Zr alloys can be used as nuclear fuels, a fast reactor operation on a closed fuel cycle will, due to nuclear reactions, contain an amount of minor actinides (Np, Am, and Cm) [3, 4]. Indeed, as was mentioned in Ref. [4], Pu-U-Zr based metallic fuel is one of the possible candidates to transmute minor actinides that can be recovered from the high-level waste by pyroprocess. This is why the principal goal of fast spectrum breeder reactors is to achieve high burn-up rates by fissioning all types of transuranic elements with complete transmutation of long-lived and high-heat-producing minor actinides, thus closing the nuclear fuel cycle with future disposition of the nuclear fuel waste products in a single geological repository [5].

Even though the thermal conductivity of Pu-U-Zr alloys is one of the highest among nuclear fuels, the radial temperature gradient generated in fast breeder reactors appears to be sufficiently large to cause redistribution of the alloy constituents [6, 7]. This redistribution alters alloy composition during irradiation, which affects local power production, variation in fission product generation, irradiation behavior such as fuel swelling and growth, and raises the question about low-melting phase precipitation. The

constituent redistribution in Pu-U-Zr alloys was studied in numerous publications [6-9] but far less attention was devoted to understand the redistribution of minor actinides [3, 4]. It is believed that a small addition of minor actinides does not alter the redistribution characteristics of Pu, U, and Zr in Pu-U-Zr fuels, and Am redistribution is similar to that of Zr: Am migrates from the Zr-depleted intermediate zone ($\gamma + \zeta$ mixture) to the hotter highly Zr-enriched porous central zone (γ-phase) and then to the colder slightly Zr-enriched porous zone ($\delta + \zeta$ mixture) on the periphery [4]. In contrast, the Np composition remains almost constant in all three zones (no redistribution or precipitation) resembling the Pu composition behavior with a slight decrease toward the fuel surface [3, 4].

Semi-empirical model calculations [6], supported by experimental observations, indicate that the excess enthalpy of solution of the γ-U-Zr phase controls the constituent redistribution process. In our previous papers [1, 2], we performed detailed calculations of the heat of formation of γ-Pu-U-Zr solid solutions. In the present study we report results of similar calculations for γ-Pu-Np, γ-Pu-Am, and γ-Pu-Cm alloys that can be used for further analysis of the constituent redistribution in the central zone of Pu-U-Zr nuclear fuels. We believe that our results are essential because experimental data on alloys that Pu forms with the minor actinides are sparse or lacking.

For our calculations we employ two complementary computational techniques: (i) the fully-relativistic (FR) exact muffin-tin orbital method (EMTO) and (ii) the full-potential linear muffin-tin orbital method (FPLMTO) that also accounts for all relativistic effects. Pertinent details of the computational methods are described in Section 2. Results of the density-functional calculations of the ground-state properties of the γ-Pu-U, γ-Pu-

Np, γ-Pu-Am, and γ-Pu-Cm solid solutions are presented in Section 3. We provide discussion in Section 4. Lastly, concluding remarks are presented in Section 5.

2. Computational details

The calculations we have referred to as EMTO are performed using the fully-relativistic spin-polarized Green function technique based on the improved screened KKR method, where the one-electron potential is represented by optimized overlapping muffin-tin (OOMT) potential spheres [10, 11]. Inside the potential spheres the potential is spherically symmetric, and it is constant between the spheres. The radii of the potential spheres, the spherical potentials inside the spheres, and the constant value in the interstitial region are determined by minimizing (i) the deviation between the exact and overlapping potentials, and (ii) the errors caused by the overlap between the spheres. Within the EMTO formalism, the one-electron states are calculated exactly for the OOMT potentials. As an output of the EMTO calculations, one can determine self-consistent Green's function of the system and the complete, non-spherically symmetric charge density. Finally, the total energy is calculated using the full charge-density technique [12]. The calculations are performed for a basis set including valence *spdf* orbitals. For the electron exchange and correlation energy functional, the generalized gradient approximation (GGA) is considered [13]. Integration over the Brillouin zone is performed using the special *k*-point technique [14] with 506 points in the irreducible wedge of the zone for the bcc structure. The moments of the density of states, needed for the kinetic energy and valence charge density, are calculated by integrating the Green function over a complex energy contour (with a 2.5 Ry diameter) using a Gaussian

integration technique with 30 points on a semi-circle enclosing the occupied states. A previous study [2] revealed that relativistic effects are important for Pu-containing systems. Because of this we use the Green function technique, based on the EMTO formalism, which includes the spin-obit coupling through the four-component Dirac equation [15].

In order to treat compositional disorder the EMTO method is combined with the coherent potential approximation (CPA) [16, 17]. The ground-state properties of the chemically random Pu-U, Pu-Np, Pu-Am, and Pu-Cm alloys are obtained from FR-EMTO-CPA calculations that include the Coulomb screening potential and energy [18-20]. The screening constants are determined from supercell calculations using the locally self-consistent Green function (LSGF) method [21] for a 1024 atoms supercell that model the random equiatomic alloys. The α and β screening constants (see Refs. [18, 19] for details) are found to be 0.93 and 1.17, 1.02 and 0.91, 1.14 and 1.00, and 1.10 and 1.00, for the bcc Pu-U, Pu-Np, Pu-Am, and Pu-Cm alloys, respectively. For the face-centered cubic (fcc) Pu-Am alloy, which was also studied in this paper, the α and β screening constants are found to be 1.07 and 1.00, respectively.

The Pu-U, Pu-Np, Pu-Am, and Pu-Cm alloys have been modeled within the disordered local moment approximation that leads to a paramagnetic solution, see Ref. [22] for details. The equilibrium atomic density of these alloys is obtained from a Murnaghan fit to the total energy versus lattice constant curve [23].

For the elemental metals, the most accurate and fully relativistic calculations are performed using an full-potential approach where the relativistic effects, including spin-orbit coupling, are accounted for. Although unable to model disorder in the CPA sense it

provides important information for the metals, and also serves to confirm the CPA calculations mentioned above. For this purpose we use a version of the FPLMTO [24-26], and the "full potential" in FPLMTO refers to the use of non-spherical contributions to the electron charge density and potential. This is accomplished by expanding the charge density and potential in cubic harmonics inside non-overlapping muffin-tin spheres and in a Fourier series in the interstitial region. We use two energy tails associated with each basis orbital, and for U's semi-core *6s*, *6p* states and valence states (*7s*, *7p*, *6d*, and *5f*) these pairs are different. With this 'double basis' approach we use a total of six energy tail parameters and a total of 12 basis functions per atom. Spherical harmonic expansions are carried out up to l_{max}= 6 for the basis, potential, and charge density. As in the case of the EMTO method, GGA is used for the electron exchange-correlation approximation. A special quasi-random structure (SQS) method, utilizing a 16-atom supercell, was used to treat the compositional disorder within the FPLMTO formalism [27]. Spin polarization for the Pu-containing alloys was arranged in an antiferromagnetic fashion [28] with neighboring atoms having anti-parallel spins. This is different from the spin configuration used in the EMTO calculations.

3. Ground-state properties of the bcc Pu-U, Pu-Np, Pu-Am and Pu-Cm solid solutions

Figure 1a shows results of FR-EMTO-CPA calculations of the heat of formation of the γ-Pu-U solid solutions at T = 0 K [2]. Notice that it is negative and in excellent agreement with data derived from a CALPHAD assessment [29-31] of the experimental thermodynamics and phase diagram information, which validates to some extent the *ab*

initio approach. Note that to have a consistent comparison between the *ab initio* and CALPHAD results, the heat of formation within CALPHAD is also taken at T = 0 K here, and in the following discussions on the Pu-Np system. For comparison, we also show the heats of formation for the $Pu_{75}U_{25}$, $Pu_{50}U_{50}$, and $Pu_{25}U_{75}$ bcc alloys, calculated within the FPLMTO-SQS technique that agrees pretty well with FR-EMTO-CPA and CALPHAD assessment.

Figure 1b shows results of FR-EMTO-CPA and FPLMTO-SQS calculations of the heat of formation of the γ-Pu-Np solid solutions at T = 0 K. In contrast to the γ-Pu-U solid solution, where the heat of formation is negative, this thermodynamic characteristic, calculated with both methods for the γ-Pu-Np solid solutions, is positive in agreement with the CALPHAD assessment [32], which is purely (no input from experimental data) based on the Brewer valence bond model [33]. Notice that the heat of formation calculated with both FR-EMTO-CPA and FPLMTO-SQS methods shows an identical asymmetry with respect to the equiatomic composition. The CALPHAD assessment, however, suggests that the heat of formation of the γ-Pu-Np solid solutions is almost symmetric with respect to the equiatomic composition. We will address the reason for this disagreement below.

Figure 1c shows results of FR-EMTO-CPA and FPLMTO-SQS calculations of the heat of formation of the γ-Pu-Am solid solutions at T = 0 K. There is an excellent agreement between results obtained from the theoretical methods. Moreover, due to the lack of experimental information and therefore a reliable CALPHAD assessment for this system, our theoretical results serve as predictions.

For the same reason it is also not possible to perform a CALPHAD assessment of the heat of formation of the γ-Pu-Cm solid solutions. Both FR-EMTO-CPA and FPLMTO-SQS calculations reveal a positive heat of formation for this system with a significant asymmetry towards the Pu-rich part of the phase diagram shown in Figure 1d. However, as was in the case of the γ-Pu-Np alloys, there is a difference in the absolute values of the heat of formation calculates with FR-EMTO-CPA and FPLMTO-SQS methods.

Figure 2 shows results of FR-EMTO-CPA calculations of the equilibrium atomic volume of the γ-Pu-U [2], γ-Pu-Np, γ-Pu-Am, and γ-Pu-Cm alloys at T = 0 K. There is a significant negative deviation from Vegard's law for the γ-Pu-U solid solution that agrees well with the negative formation energy of these alloys. Our calculations show that there is also a negative deviation from the Vegard's law for the γ-Pu-Np solid solution, although to a lesser extent than in the case of the γ-Pu-U alloys, resulting in a slightly positive heat of formation. However, the calculated value of the equilibrium volume of pure γ-Np is significantly smaller than observed experimentally [34] causing a significant error in the volume vs. alloy composition profile for this system. The inability to describe the high-temperature γ-phase of Np within the zero temperature DFT formalism causes an error in the energy of formation of γ-Pu-Np solid solution as can be seen in Figure 1b.

Finally, there is a positive deviation from Vegard's law for the equilibrium volume calculated for the γ-Pu-Am and γ-Pu-Cm alloys, shown in Figures 2c and 2d, respectively, which is in accord with the positive heat of formation in these systems. There is no experimental information on the equilibrium volume of the bcc Pu-Am solid solutions. However, the positive deviation from Vegard's law is experimentally found in

the fcc Pu-Am alloys [35]. Results of FR-EMTO-CPA calculations of the equilibrium atomic volume of the fcc Pu-Am alloys at T = 0 K are presented in Figure 3 which are in good accord with the experimental data [35]. Results of FR-EMTO-CPA calculations of the heat of formation of the fcc and bcc Pu-Am solutions are compared in Figure 4. The heat of formation for the fcc Pu-Am solid solutions is also positive, which is in accord with the experimentally observed positive deviation from Vegard's law shown in Figure 3, but smaller that of the bcc Pu-Am solid solutions. This is why we can conclude that the continuous fcc Pu-Am solid solutions, formed by fcc δ-Pu and β-Am, can exist at low temperatures, but at higher temperatures the continuous bcc γ-Pu-Am solid solutions can be formed by bcc ε-Pu and γ-Pu – the phase sequence that was suggested in the so-called "Russian" version of the Pu-Am phase diagram [36].

4. Discussion

In Figure 5 we compared the results of FR-EMTO-CPA calculations of the heat of formation of the bcc Pu-U, Pu-Np, Pu-Am, and Pu-Cm solid solutions. The insert shows the charge transfer on the Pu atoms, ΔQ_{Pu}, calculated by the LSGF method [21] for a 1024 atoms supercell that models the random equiatomic alloy. The sign of the charge transfer on Pu atoms is positive when the dopant element (U or Np) is located to the left from Pu in the actinide row (has a smaller Wigner-Seitz radius) or negative when the dopant element (Am or Cm) is located to the right in the actinide row (has a larger Wigner-Seitz radius). According to Ref. [19], the Madelung energy contribution to the formation energy of the disordered alloy is proportional to $(-\alpha \frac{\Delta Q^2}{S_{ws}})$, where α is the

screening constant and S_{WS} is the Wigner-Seitz radius, which is related to the atomic volume, Ω, through $\Omega = \frac{4\pi S_{WS}^{3}}{3}$. Thus, as the absolute value of the charge transfer on the Pu atoms, ΔQ_{Pu}, decreases along the actinide row U→Np→Am→Cm, the formation energy of the alloy increases that is actually found by present calculations for the sequence of the Pu-U→Pu-Np→Pu-Am alloys. The largest positive heat of formation should be observed in the Pu-Cm system that has the smallest magnitude of the charge transfer among the alloys under consideration. This, indeed, should explain why only ~ 1 at. % of Cm can be dissolved in ε-Pu [37]. However, present calculations not only fail to justify a very limited solubility of Cm in bcc Pu (the formation energy is not large enough), but also shows a significant decrease of the formation energy in the γ-Pu-Cm alloys as composition of Cm exceeds 20 at. %.

Among the Pu-based bcc solid solutions studied in this paper the γ-Pu-U system has a negative formation energy that is accompanied by a significant negative deviation for the equilibrium atomic volume from Vegard's law. This deviation for the molar volume of the liquid Pu-U alloys was measured in Ref. [38], and alignment of the experimental solidus-liquidus curves from the case of the Pu-U phase diagram [39] indicated that a similar tendency should be observed in the case of the bcc Pu-U solid solutions. The excellent agreement between the results of FR-EMTO-CPA calculations of the heat of formation of γ-Pu-U solid solutions and data derived from a CALPHAD assessment is mostly due to the correct description of the charge transfer that occurs between the constituents of this system. A significant charge transfer causes a large negative interaction term that was introduced in Ref. [32] in order to explain the

experimental liquidus and solidus in the Pu-U system. If this contribution is not taken into account, the Brewer valence bond model [33], used in Ref. [32], fails to describe the solid-liquid equilibrium in this system.

In the case of the γ-Pu-Np and γ-Pu-Am alloys the energy of formation becomes positive that is reflected in our calculations. Our FR-EMTO-CPA treatment gives ~ 30 % error for the maximum value of the heat of formation of the γ-Pu-Np solid solutions in comparison with a CALPHAD assessment of this thermodynamic property [32] based on the Brewer valence bond model. The situation is different in the case of γ-Pu-Am alloys. Except for some rough estimates of the heat of formation of the fcc and bcc Pu-Am alloys [32], based on the Brewer valence bond model, and a CALPHAD assessment [40], *ab initio* calculations of this property for the Pu-Am system have never been performed. The so-called "American" version of the Pu-Am phase diagram [35] was constructed on the assumption that only two allotropes of Am: α-Am (double-hexagonal close-packed or dhcp) and β-Am (fcc) existed with a limited solubility of about 8 at. % Am in ε-Pu. We believe that the present FR-EMTO-CPA heat of formation of the fcc and bcc Pu-Am solid solution will not only help to confirm the so-called "Russian" version of the Pu-Am phase diagram [36], which assumes existence of the γ-Am (bcc) allotropy and continuous fcc and bcc solid solution, but also help in the estimation of Am redistribution in the Pu-U-Zr metallic fuels for fast breeder reactors. To perform the later task one also needs information on the heat of formation of the bcc U-Am and Zr-Am solid solutions that can be calculated within FP-EMTO-CPA formalism. The results of these calculations will be presented in our future publication.

5. Conclusion

In the present paper *ab initio* results are obtained for the Pu-U, Pu-Np, Pu-Am, and Pu-Cm alloys to understand the effectiveness of first-principle methods in describing actinide alloys. Ground-state properties of the bcc Pu-U, Pu-Np, Pu-Am, and Pu-Cm solid solutions were calculated. These *ab initio* results will be used to build a thermodynamic database with important input from first-principles theory that will be directly comparable to the results obtained solely from experimental data on thermodynamic properties and phase diagrams. Since the amount of minor actinides, especially Am, in the Pu-U-Zr metallic fuels for fast breeder reactors may be significant, it is important to include the above listed calculated ground-state properties in a thermodynamic database dedicated to these fuels in order to understand the constituent redistribution process caused by the radial temperature gradient generated in these reactors, including the impact that minor actinides put on the stability properties and performance of metallic fuels.

Acknowledgements

This work was performed under the auspices of the U.S. Department of Energy by Lawrence Livermore National Laboratory under contract DE-AC52-07NA27344. Support from the Swedish Research Council (VR) is gratefully acknowledged by LV, OEP, and AVR.

References:

1. A. Landa, P. Söderlind, P.E.A. Turchi, L. Vitos, A. Ruban, J. Nucl. Mater. 385 (2009) 68-71.
2. A. Landa, P. Söderlind, P.E.A. Turchi, L. Vitos, A. Ruban, J. Nucl. Mater. 393 (2009) 141-145.
3. M. Kurata, T. Inoue, C. Sari, J. Nucl. Mater. 208 (1994) 144-158.
4. Yeon Soo Kim, G.L. Hofman, S.L. Hayes, Y.H Sohn, J. Nucl. Mater. 327 (2004) 27-36.
5. D.D. Keiser Jr., J.B. Kennedy, B.A. Hilton, S.L. Hayes, JOM № 1 (2008) 29-32.
6. G.L. Hofman, S.L. Hayes, M.C. Petri, J. Nucl. Mater. 227 (1996) 277-286.
7. G.L. Hofman, L.C. Walters, T.H. Bauer, Progr. Nucl. Energy 31 № 1/2 (1997) 83-110.
8. Y.H. Sohn, M.A. Dayananda, G.L. Hofman, R.V. Strain, S.L. Hayes, J. Nucl. Mater. 279 (2000) 317-329.
9. Yeon Soo Kim, S.L. Hayes, G.L. Hofman, A.M. Yacout, J. Nucl. Mater. 359 (2006) 17-28.
10. L. Vitos, Phys. Rev B 64 (2001) 014107-1-11.
11. L. Vitos, Computational Quantum Mechanics for Materials Engineers: The EMTO Method and Application, Springer, London, 2007.
12. J. Kollar, L. Vitos, H.L. Skriver, in: H. Dreyssé (Ed.), Electronic Structure and Physical Properties of Solids: The Uses of the LMTO Method, Lecture Notes in Physics, Springer, Berlin, 2000, pp. 85-113.
13. J.P. Perdew, K. Burke, M. Ernzerhof, Phys. Rev. Lett. 77 (1996) 3865-3868.

14. D.J. Chadi, M.L. Cohen, Phys. Rev. B 8 (1973) 5747-5753; Phys. Rev B 39 (1989) 3168-3172.
15. L. V. Pourovskii, A. V. Ruban, L. Vitos, H. Ebert, B. Johansson, I. A. Abrikosov, Phys. Rev. B 71 (2005) 094415-1-10.
16. J.S. Faulkner, Prog. Mater. Sci. 27 (1982) 1-187.
17. L. Vitos, I.A. Abrikosov, B. Johansson, Phys. Rev. Lett. 87 (2001) 156401-4.
18. A.V. Ruban, H.L. Skriver, Phys. Rev. B 66 (2002) 024201-1-15.
19. A.V. Ruban, S.I. Simak, P.A. Korzhavyi, H.L. Skriver, Phys. Rev. B 66 (2002) 024202-1-12.
20. A.V. Ruban, S.I. Simak, S. Shallcross, H.L. Skriver, Phys. Rev. B 67 (2003) 214302-1-12.
21. I.A. Abrikosov, S.I. Simak, B. Johansson, A.V. Ruban, H.L. Skriver, Phys. Rev. B 56 (1997) 9319-9334.
22. P. Söderlind, A. Landa, B. Sadigh, Phys. Rev. B 66 (2002) 205109-1-6; A. Landa, P. Söderlind, J. Alloys Comp. 354 (2003) 99-103.
23. F.D. Murnaghan, Proc. Natl. Acad. Sci. U.S.A. 30 (1944) 244-247.
24. J.M. Wills, B. Cooper, Phys. Rev. B 36 (1987) 3809-3823.
25. D.L. Price, B. Cooper, Phys. Rev. B 39 (1989) 4945-4957.
26. J.M. Wills, O. Eriksson, M. Alouani, D.L. Price, in: H. Dreyssé (Ed.), Electronic Structure and Physical Properties of Solids: The Uses of the LMTO Method, Lecture Notes in Physics, Springer, Berlin, 2000, pp.148-167.
27. A. Zunger, S.H. Wei, L.G. Ferreira, J.E. Bernard, Phys. Rev. Lett. 65 (1990) 353-356.

28. P. Söderlind, B. Sadigh, Phys. Rev. Lett. 92 (2004) 185702-1-4; P. Söderlind, Europhys. Lett. 55 (2001) 525-531.
29. P.E.A. Turchi, I.A. Abrikosov, B. Burton, S.G. Fries, G. Grimvall, L. Kauffman, P. Korzhavyi, V. Rao Manga, M. Ohno, A. Pisch, A. Scott, W. Zhang, CALPHAD 31 (2007) 4-27.
30. M. Kurata, T. Ogata, K. Nakamura, T. Ogawa, J. Alloys Comp. 271/273 (1998) 636-640.
31. M. Kurata, CALPHAD 23 (1999) 315-337.
32. T. Ogawa, J. Alloys Compd. 194 (1993) 1-7.
33. L. Brewer, R.H. Lamoreaux, At. Energy Rev., Spec. Issue № 7 (1980) 11-194.
34. P.G. Mardon, J. H. Pearce, J.A.C. Marples, J. Less-Common Met. 3 (1961) 281-292.
35. F.H. Ellinger, K.A. Johnson, V.O. Struebing, J. Nucl. Mater. 20 (1966) 83-86.
36. V.D. Shushakov, N.S. Kosulin, N.T. Chebotarev, *The Phase Diagram of Plutonium-Americium Alloys*, in: Questions of Atomic Science and Technology, series Material Science and New Materials, 1990 (3) 14-15.
37. V.D. Shushakov, N.T. Chebotarev, Radiochemistry 37 (1995) 446-448.
38. L.J. Wittenbereg, D. Ofte, W.G. Rohr, D.V. Rigney, Metall. Trans. 2 (1971) 287-290.
39. H. Okamoto, J. Phase Equilibria 17 (1996) 372.
40. M. Kurata, IOP Conf. Series: Materials Science and Engineering 9 (2010) 012023-1-8.

Captions

Figure 1. Heat of formation (in kJ/mole) versus composition for the γ-Pu-U (a), γ-Pu-Np (b), γ-Pu-Am (c), and γ-Pu-Cm (d) alloys (T = 0 K).

Figure 2. Atomic volume (in nm^3) versus composition for the γ-Pu-U (a), γ-Pu-Np (b), γ-Pu-Am (c), and γ-Pu-Cm (d) alloys (T = 0 K). Experimental data for the γ-Pu-Np alloys are taken from Ref. [34].

Figure 3. Atomic volume (in nm^3) versus composition for the fcc Pu-Am alloys (T = 0 K). Experimental data are taken from Ref. [35].

Figure 4. Heat of formation (in kJ/mole) versus composition for the fcc and bcc Pu-Am alloys.

Figure 5. Heat of formation (in kJ/mole) versus composition for the bcc Pu-U, Pu-Np, Pu-Am, and Pu-Cm alloys (T = 0 K). The insert shows the charge transfer on the Pu atoms calculated by the LSGF method [21] for a supercell that models the random equiatomic alloy.

Figures.

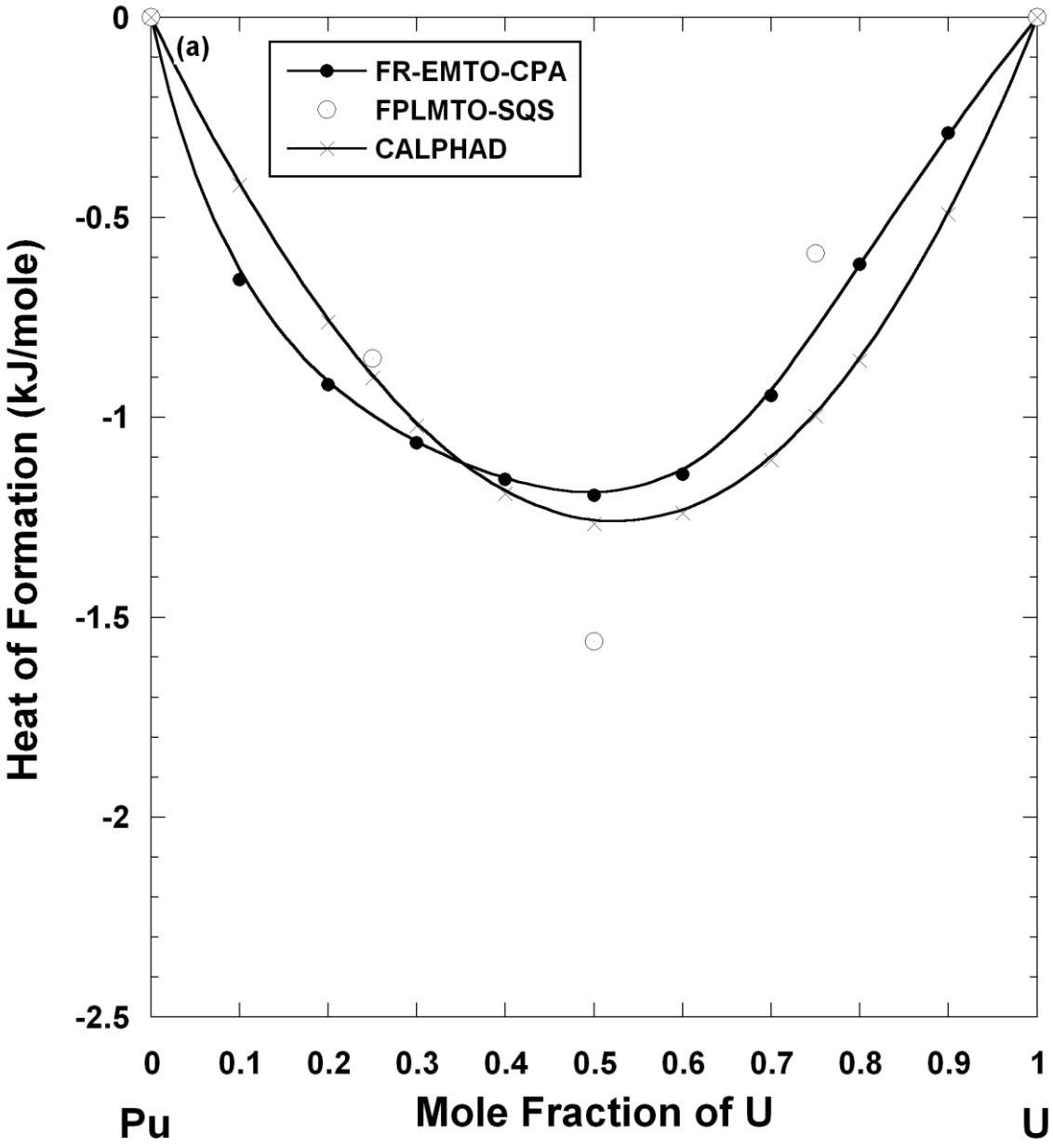

Figure 1a.

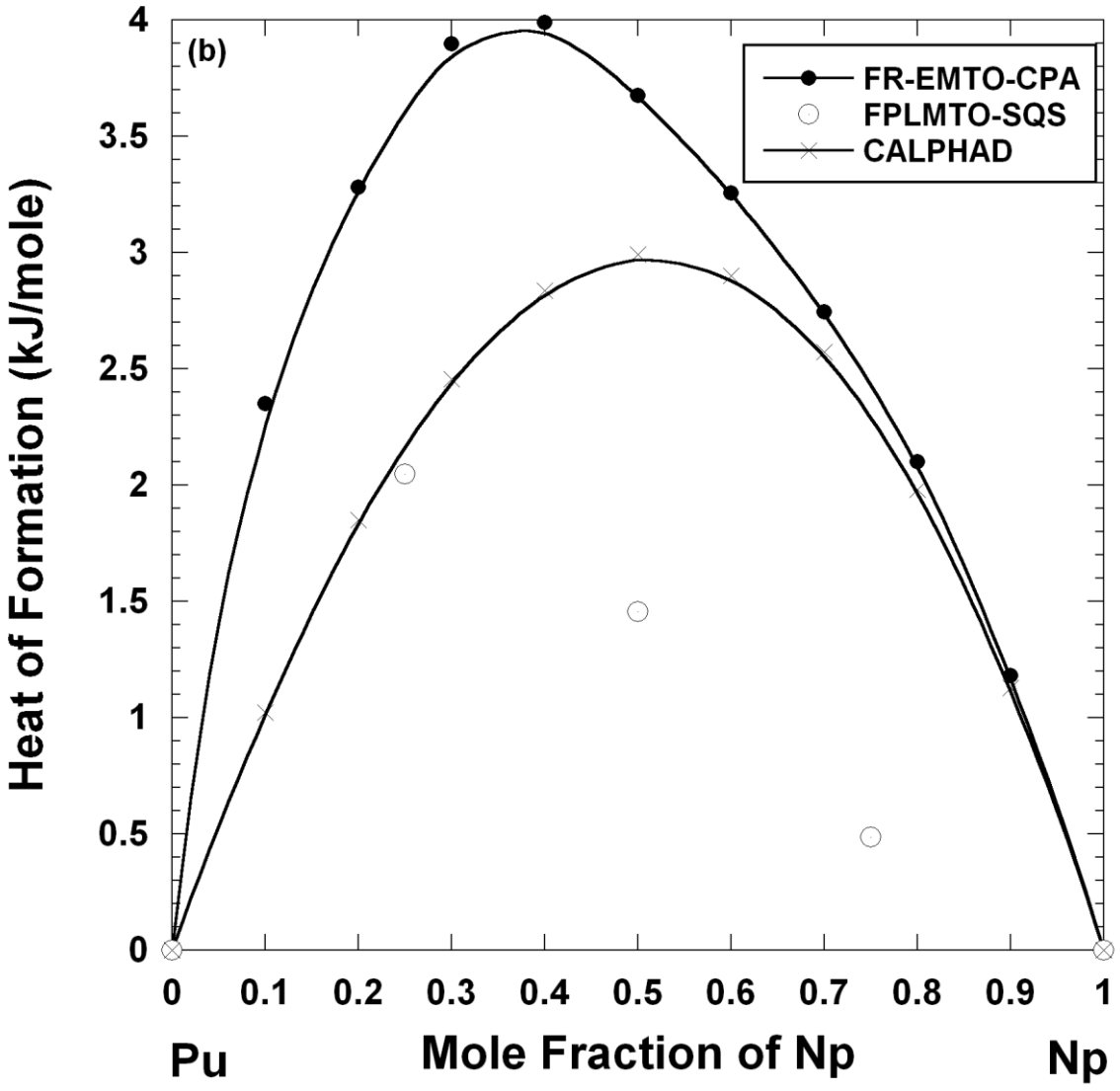
(b)
FR-EMTO-CPA
FPLMTO-SQS
CALPHAD
Heat of Formation (kJ/mole)
Mole Fraction of Np
Pu
Np
0
0.5
1
1.5
2
2.5
3
3.5
4
0
0.1
0.2
0.3
0.4
0.5
0.6
0.7
0.8
0.9
1

Figure 1b.

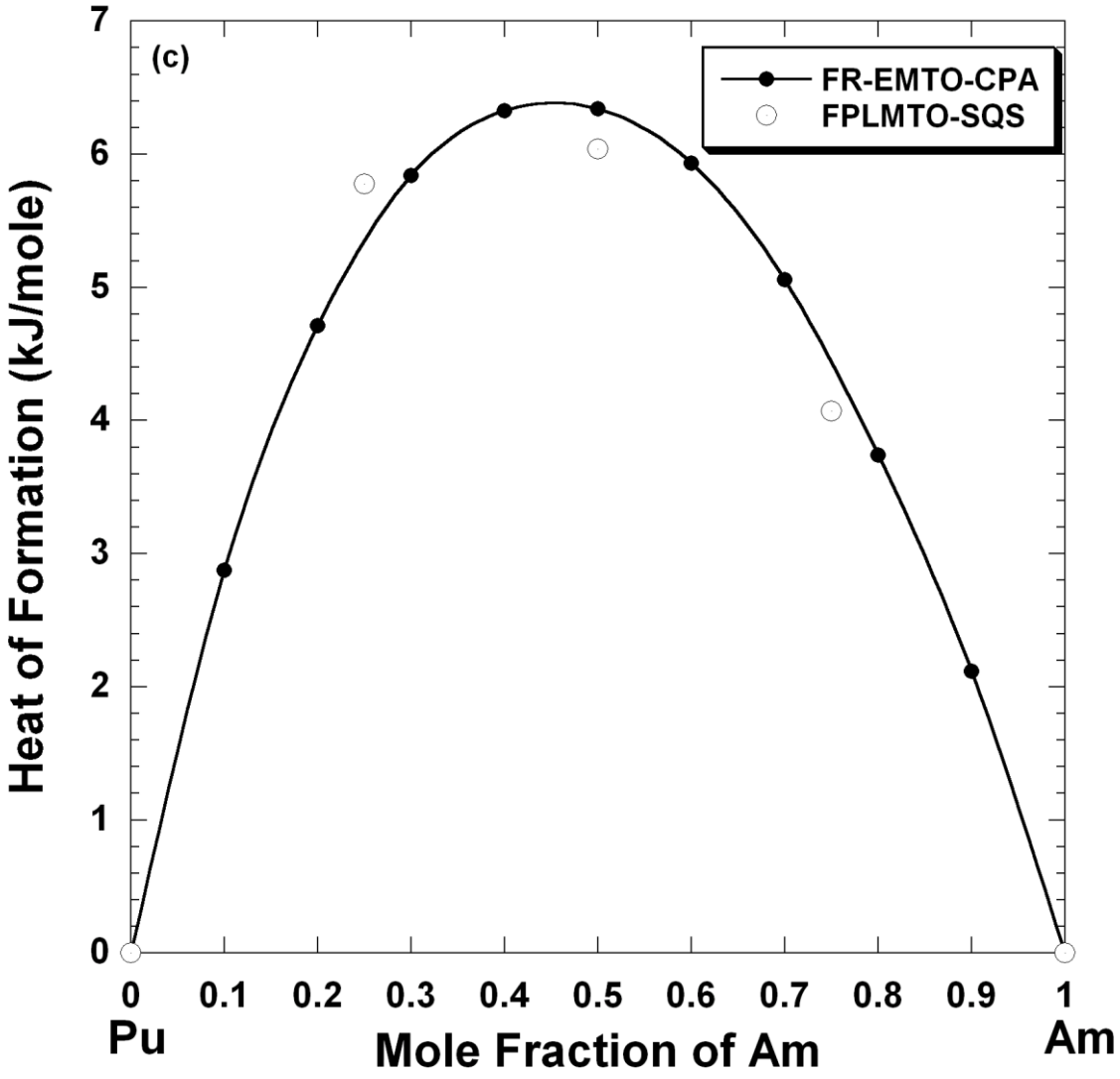
(c)
FR-EMTO-CPA
FPLMTO-SQS
Heat of Formation (kJ/mole)
0
1
2
3
4
5
6
7
0
0.1
0.2
0.3
0.4
0.5
0.6
0.7
0.8
0.9
1
Pu
Mole Fraction of Am
Am

Figure 1c.

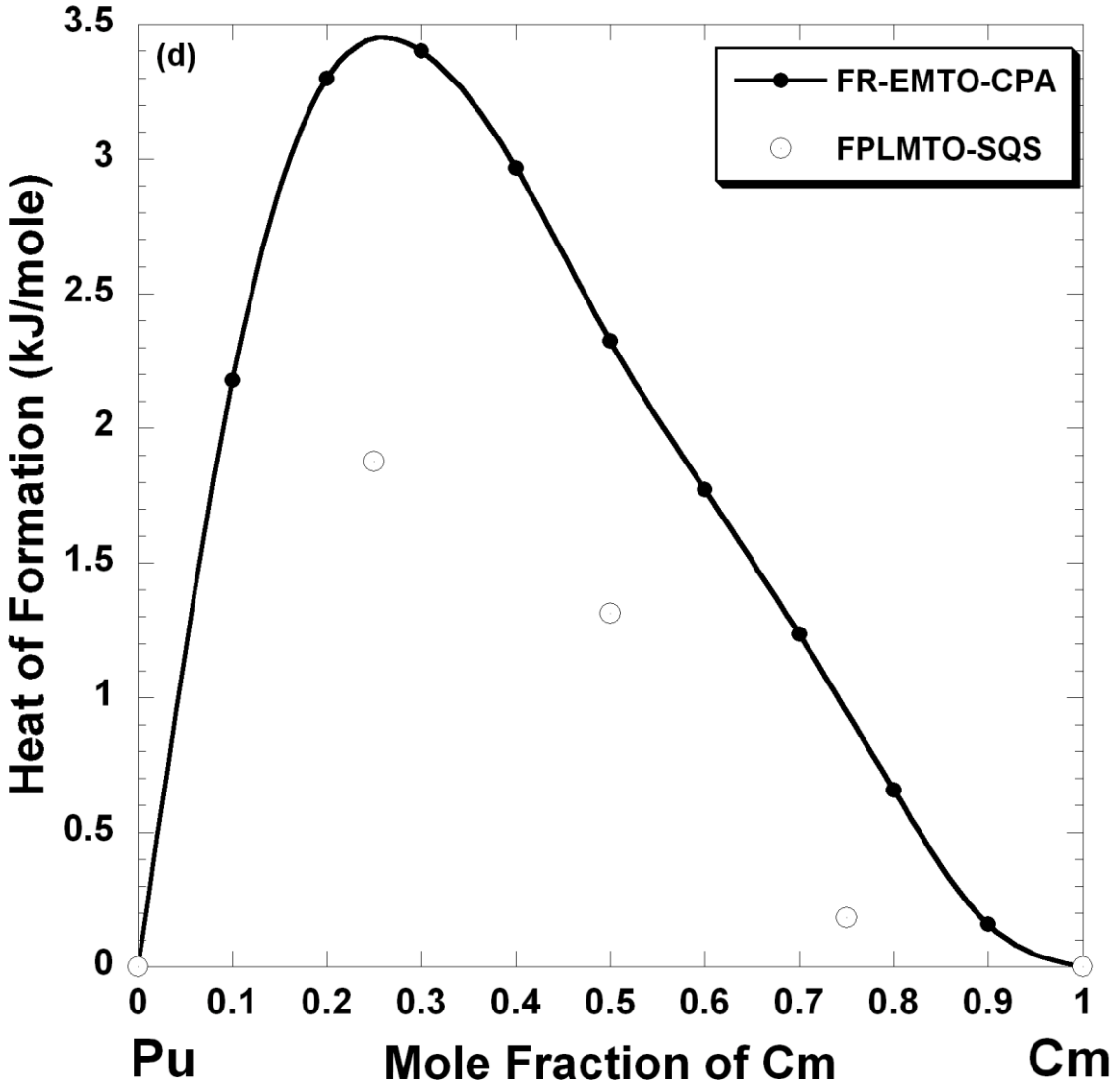
(d)
FR-EMTO-CPA
FPLMTO-SQS
Heat of Formation (kJ/mole)
3.5
3
2.5
2
1.5
1
0.5
0
0
0.1
0.2
0.3
0.4
0.5
0.6
0.7
0.8
0.9
1
Pu
Mole Fraction of Cm
Cm

Figure 1d.

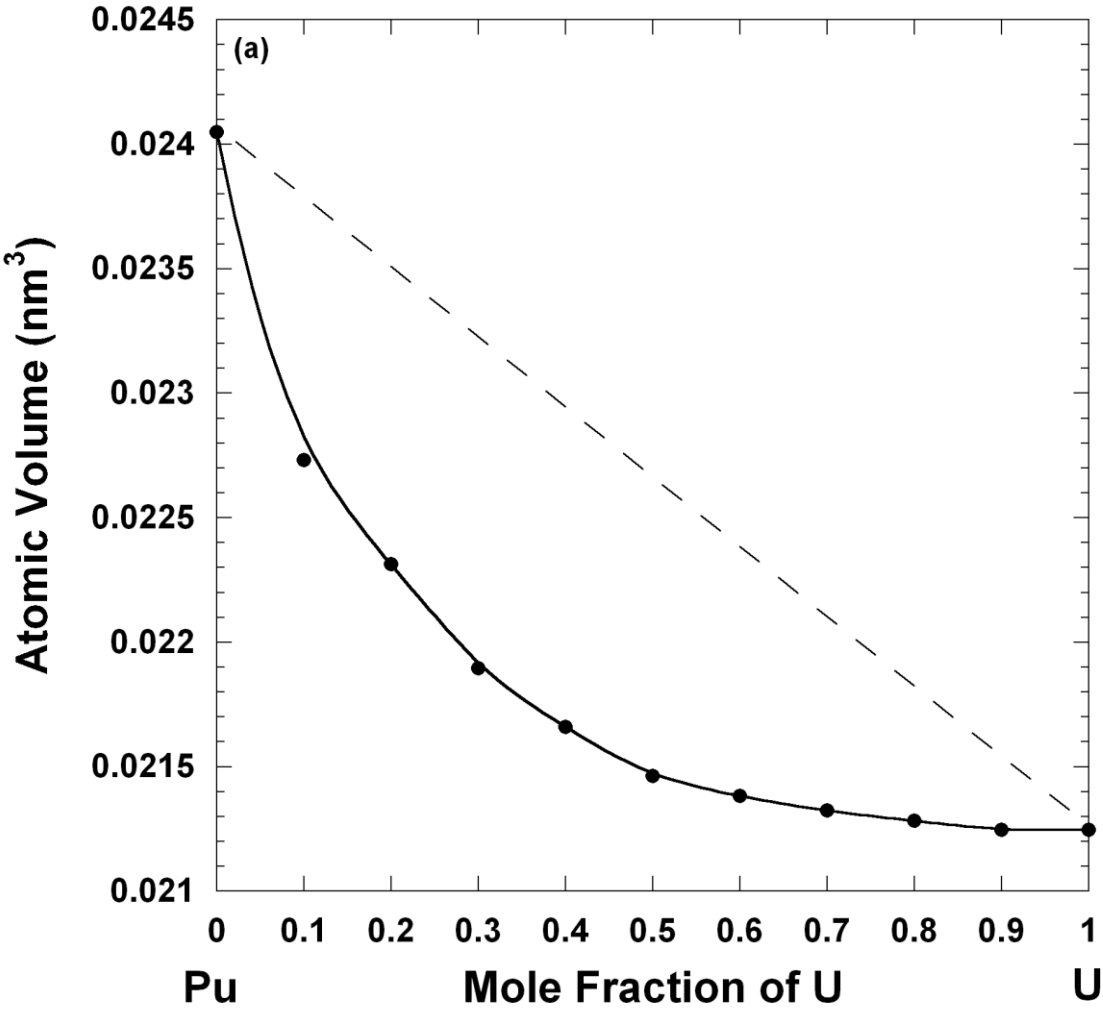
(a)
0.0245
0.024
0.0235
0.023
0.0225
0.022
0.0215
0.021
Atomic Volume (nm^3)
0
0.1
0.2
0.3
0.4
0.5
0.6
0.7
0.8
0.9
1
Pu
Mole Fraction of U
U

Figure 2a.

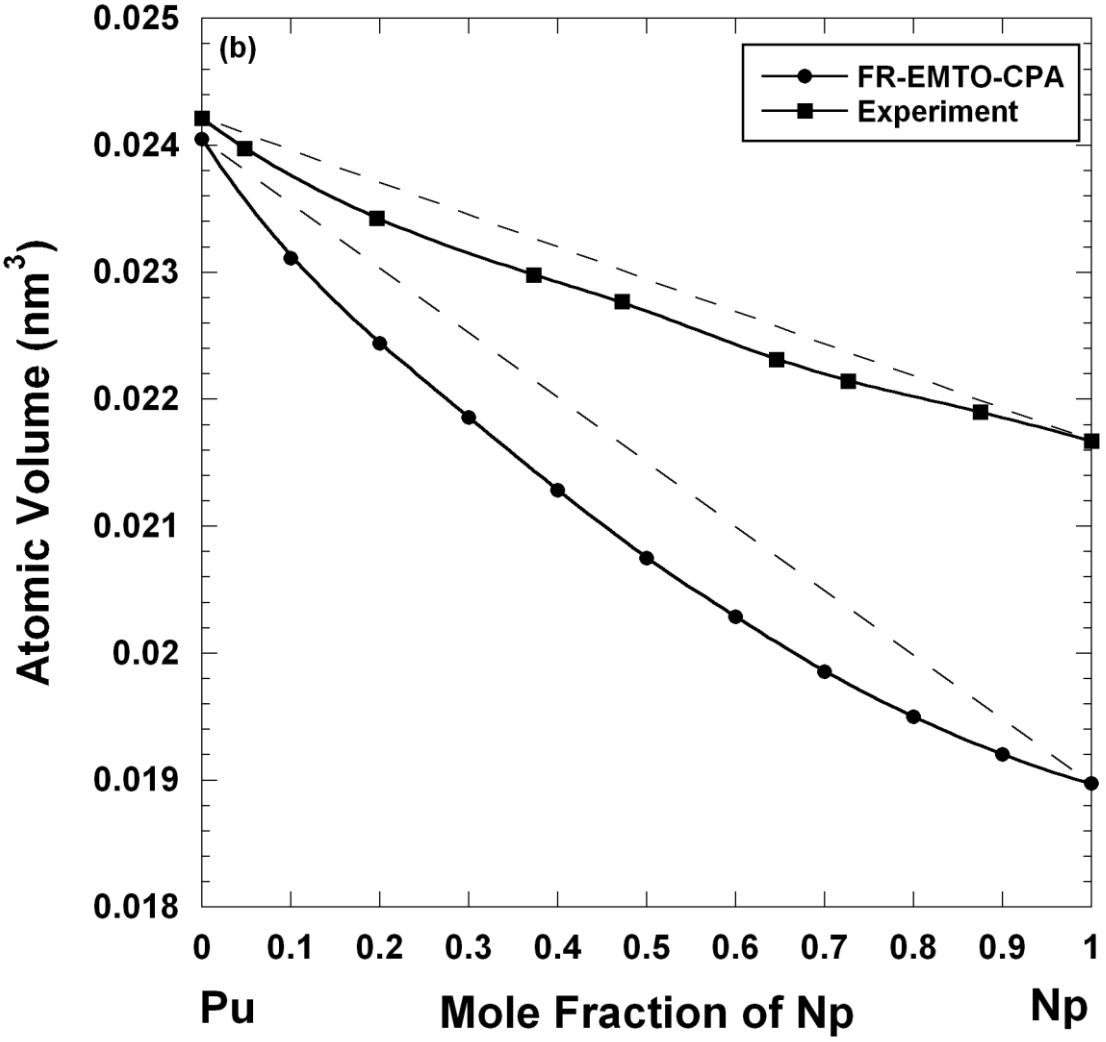
(b)
FR-EMTO-CPA
Experiment
Atomic Volume (nm^3)
0.025
0.024
0.023
0.022
0.021
0.02
0.019
0.018
0
0.1
0.2
0.3
0.4
0.5
0.6
0.7
0.8
0.9
1
Pu
Mole Fraction of Np
Np

Figure 2b.

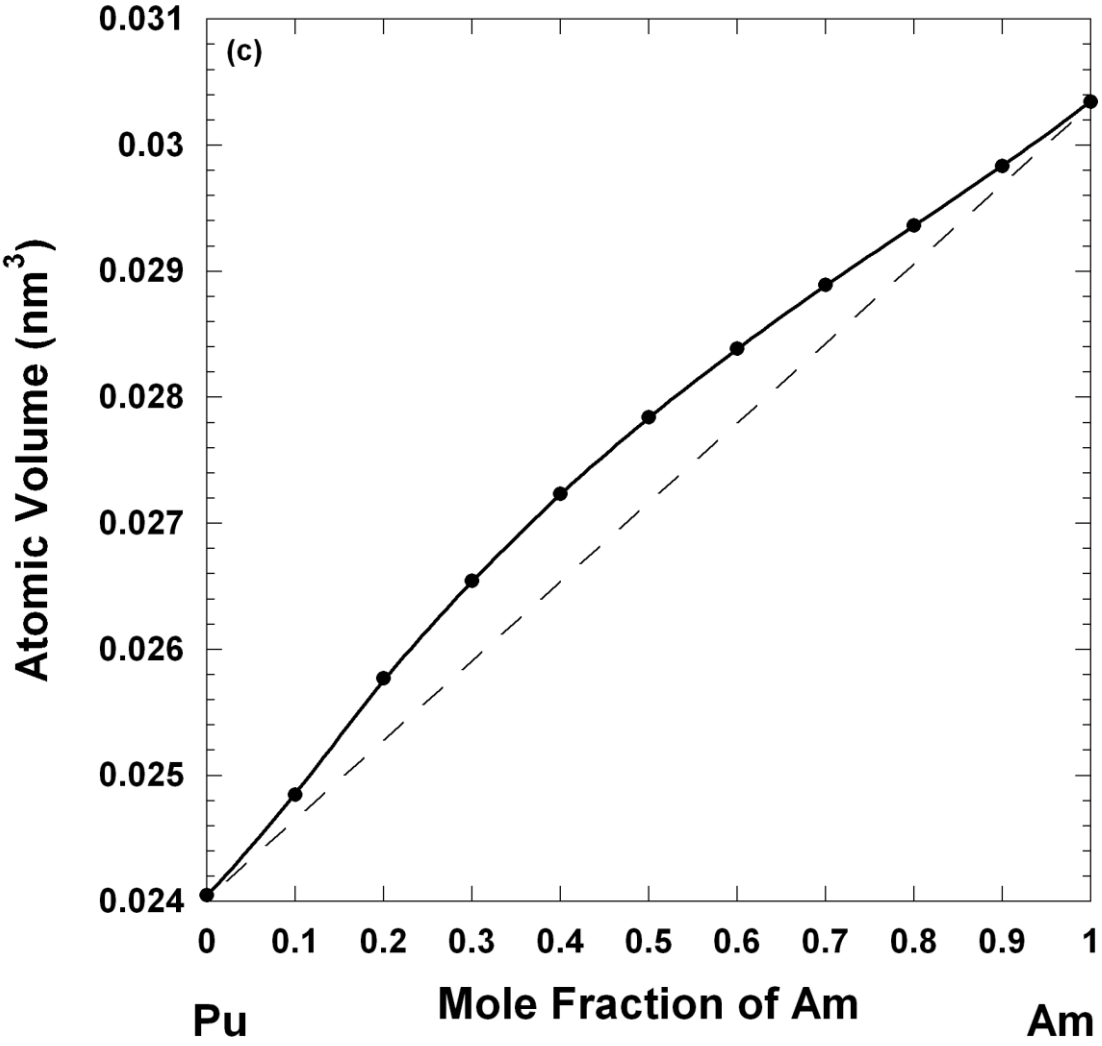
(c)
0.031
0.03
0.029
0.028
0.027
0.026
0.025
0.024
Atomic Volume (nm3)
0
0.1
0.2
0.3
0.4
0.5
0.6
0.7
0.8
0.9
1
Pu
Mole Fraction of Am
Am

Figure 2c.

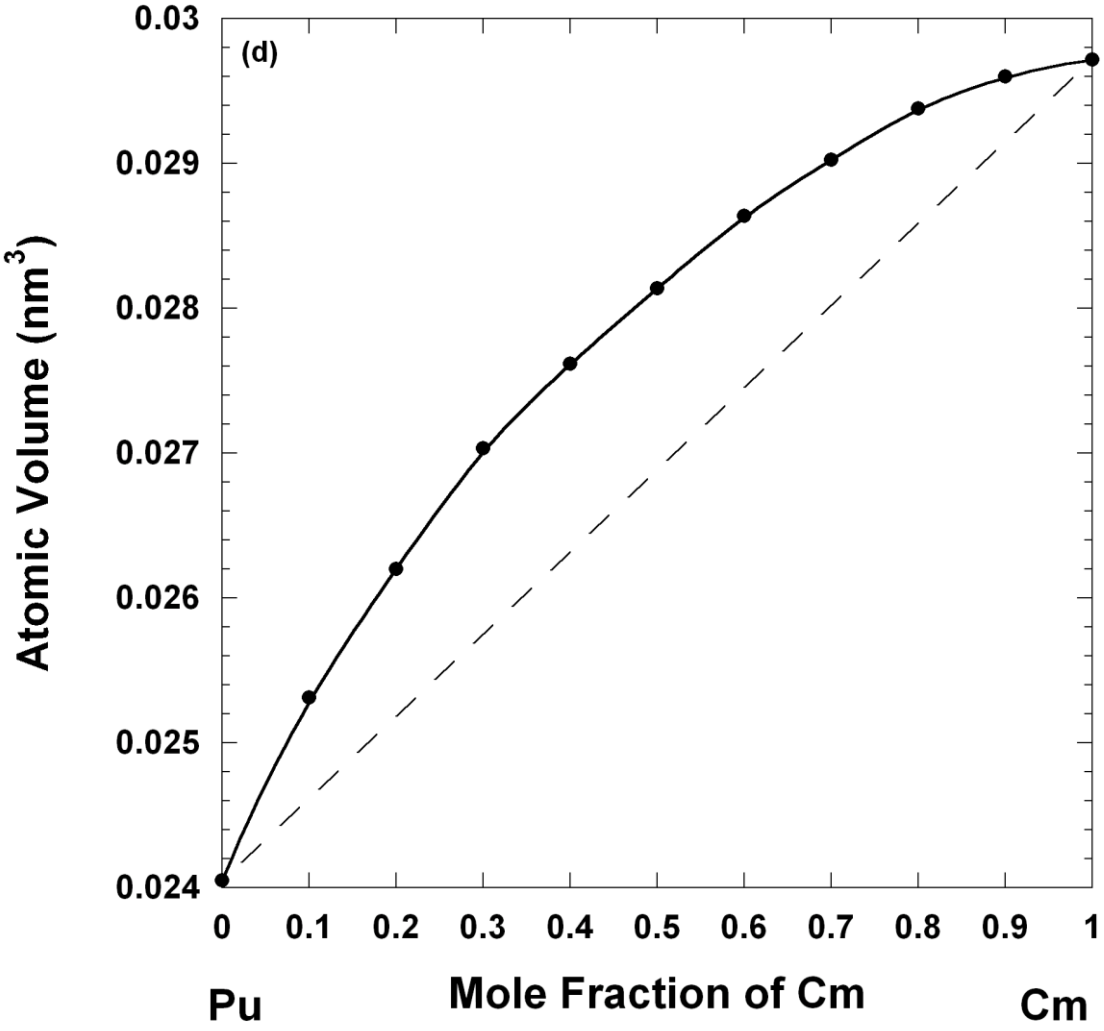
(d)
Atomic Volume (nm^3)
0.03
0.029
0.028
0.027
0.026
0.025
0.024
0
0.1
0.2
0.3
0.4
0.5
0.6
0.7
0.8
0.9
1
Pu
Mole Fraction of Cm
Cm

Figure 2d.

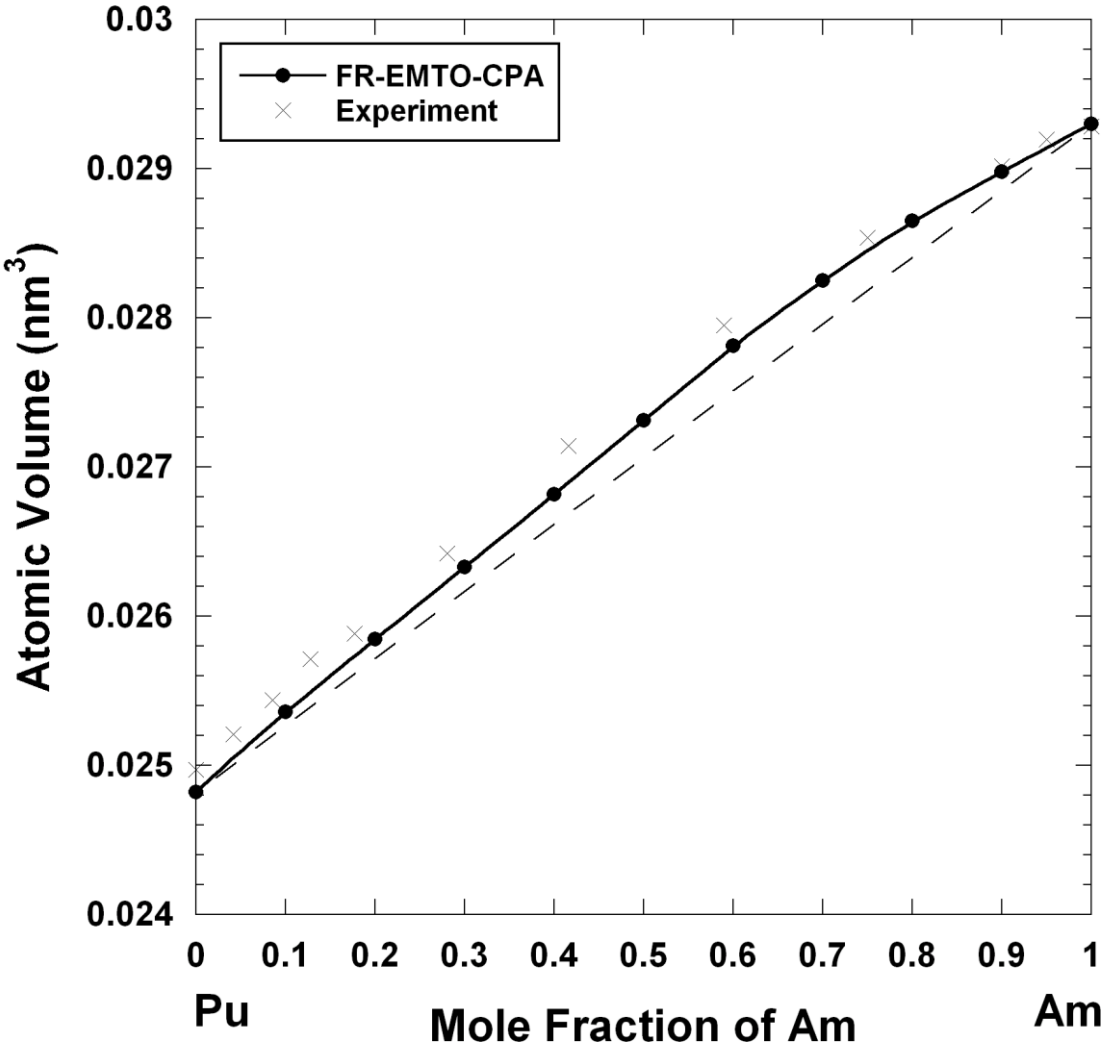
FR-EMTO-CPA
Experiment
Atomic Volume (nm^3)
0.03
0.029
0.028
0.027
0.026
0.025
0.024
0
0.1
0.2
0.3
0.4
0.5
0.6
0.7
0.8
0.9
1
Pu
Mole Fraction of Am
Am

Figure 3.

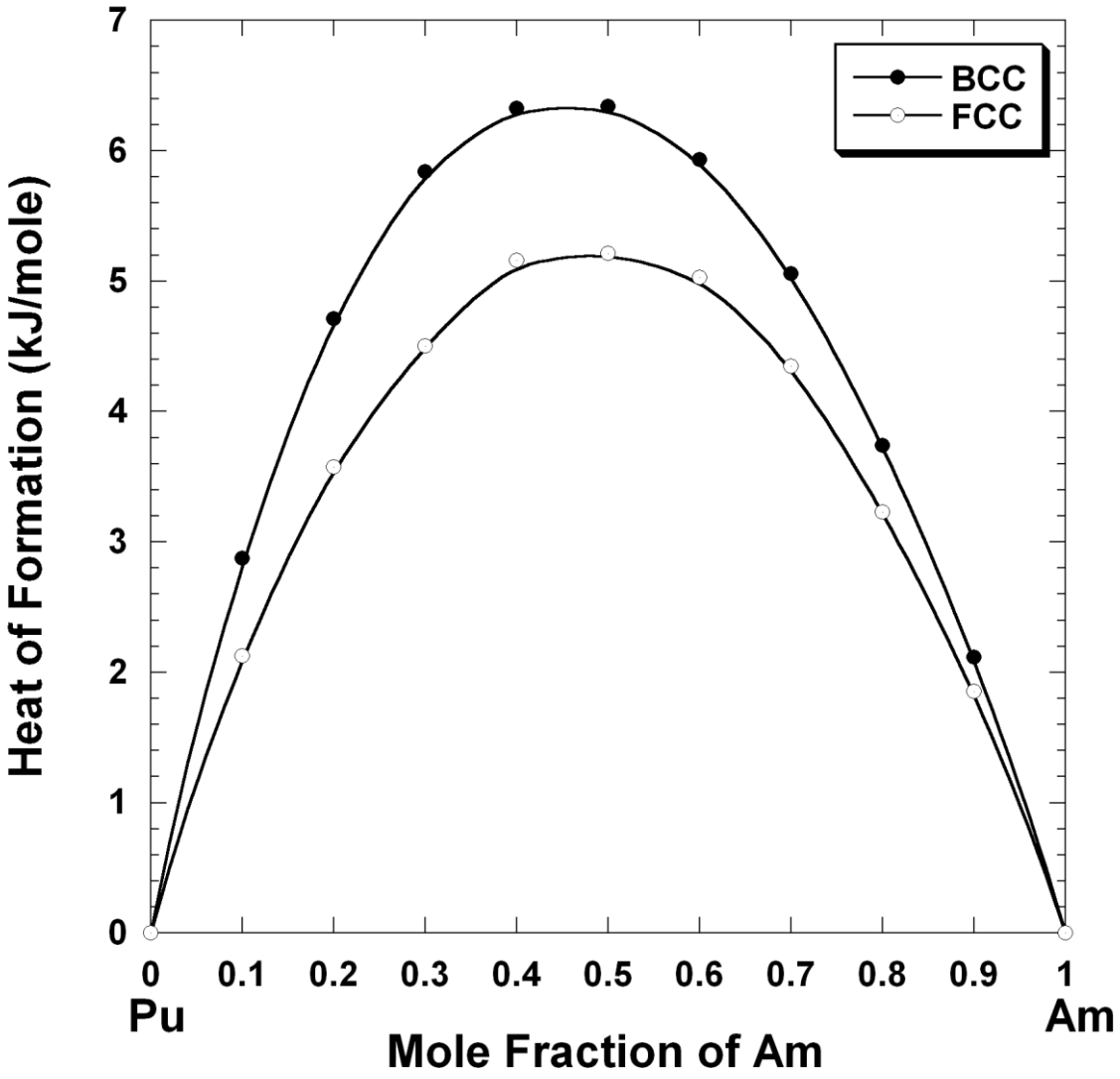
BCC
FCC
Heat of Formation (kJ/mole)
0
1
2
3
4
5
6
7
0
0.1
0.2
0.3
0.4
0.5
0.6
0.7
0.8
0.9
1
Pu
Am
Mole Fraction of Am

Figure 4.

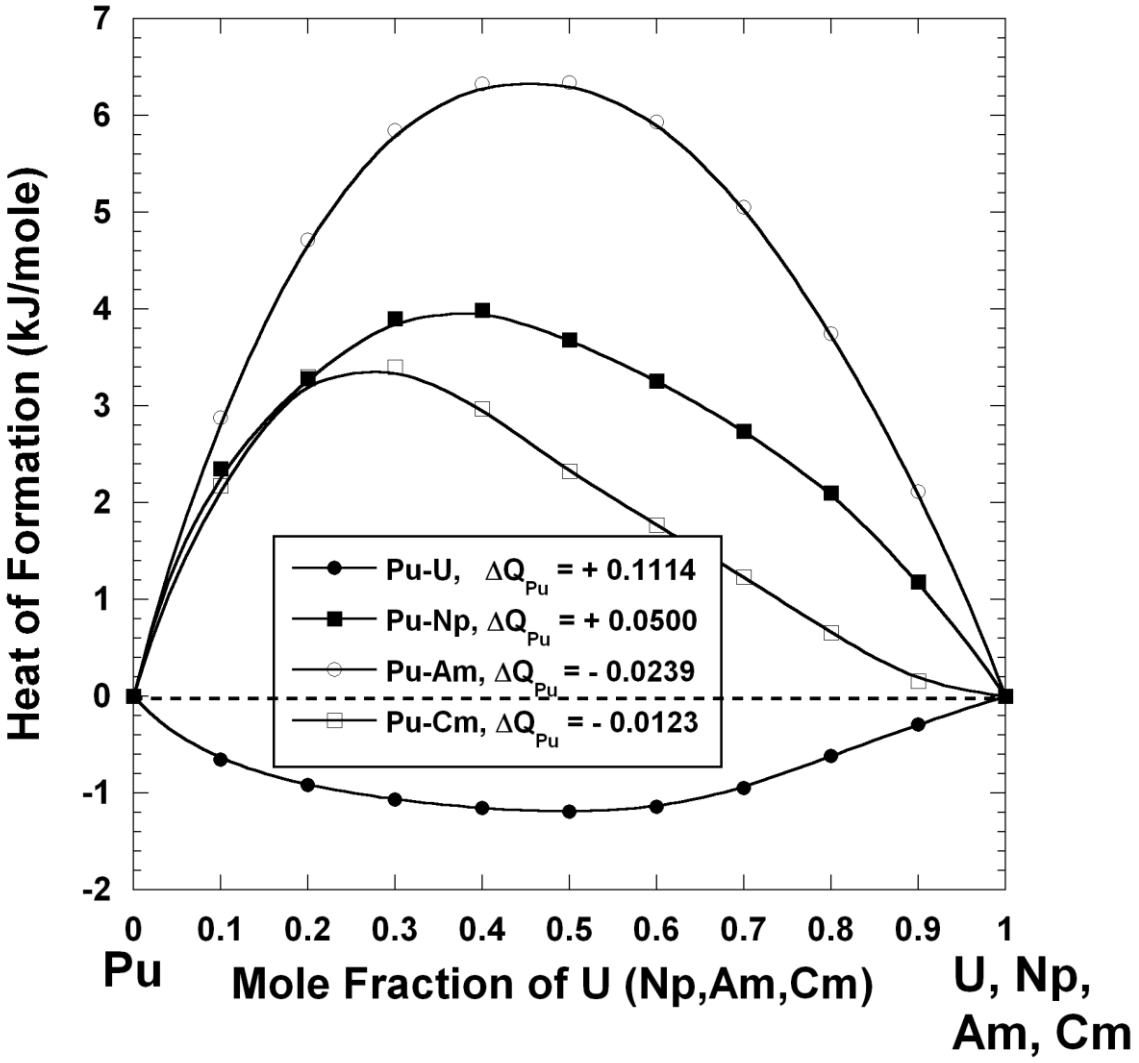
Heat of Formation (kJ/mole)
7
6
5
4
3
2
1
0
-1
-2
0
0.1
0.2
0.3
0.4
0.5
0.6
0.7
0.8
0.9
1
Pu
Mole Fraction of U (Np,Am,Cm)
U, Np, Am, Cm
Pu-U, ΔQPu = + 0.1114
Pu-Np, ΔQPu = + 0.0500
Pu-Am, ΔQPu = - 0.0239
Pu-Cm, ΔQPu = - 0.0123

Figure 5.